FEA-Based Design and Parameter Optimization Study of 6-Slot 5-Pole PMFSM with Field Excitation for Hybrid Electric Vehicle

E. Sulaiman*, T. Kosaka** and N. Matsui**
* University Tun Hussein Onn Malaysia, Johor, Malaysia. Email: erwan@uthm.edu.my
** Nagoya Institute of Technology, Nagoya, Japan. Email: kosaka@nitech.ac.jp

***Abstract*—Permanent magnet flux switching machine (PMFSM) with additional coil excitation has several attractive features compared to interior permanent magnet synchronous machines (IPMSM) conventionally employed in HEVs. The variable flux control capability and robust rotor structure make this machine becoming more attractive to apply for high speed motor drive system coupled with reduction gear. This paper presents an investigation into design possibility and parameter optimization study of 6-slot 5-pole PMFSM with hybrid excitation for traction drives in HEVs. The design target is the motor with maximum power more than 123kW and maximum power density more than 3.5kW/kg. A reduction of permanent magnet material for a given torque requirement and an extension in speed and torque ranges are chosen as the optimization indices. The designed motor enables to keep the same power density in existing IPMSM installed on a commercial SUV-HEV.**

***Keywords*— Permanent Magnet Flux Switching Machine (PMFSM); Hybrid Electric Vehicle (HEV); Field Excitation; Finite Element Analysis.**

I. INTRODUCTION

With ever increasing concerns about environmental protection and energy conservation, the use of Hybrid Electric Vehicle (HEV) for road transportation is becoming increasingly attractive. To enable HEV to directly compete with gasoline vehicles, an electric motor installed on HEV aims to pursue high efficiency, high power density, high controllability, wide speed range and maintenance-free operation [1-3].

Over the past decade, many automotive companies have been commercializing HEV in which Permanent Magnet Synchronous Motor (PMSM) using rare-earth magnet has been employed as the main traction drives. This is due to the restriction of motor size to ensure enough passenger space and the limitation of motor weight to reduce fuel consumption [4-6]. However, a dramatic increase in usage of the rare-earth magnet would cause serious problems such as increasing in the price of the rare-earth magnet, security and undersupply. Moreover, according to the report released by Mineral Resource Information Center affiliated to Japan Oil, Gas and Metals National Corporation, an increase in annual usage of rare-earth magnet, $N_{d2}F_{e14}B$, have brought about the price-up of rare-earth metals not only Neodymium (N_d) but also Dysprosium (D_y) and Terbium (T_b) which are indispensable to provide the rare-earth magnet with high coercivity as the additives. Therefore, the continuous researches and developments of non- or less-rare-earth magnet machines would be very important [7-8].

As one example of the successfully developed HEV, the historical progress in the power density of main traction motor installed on TOYOTA HEV has showed that the power density of each motor employed in LEXUS RX400h ’05 and GS450h ‘06 has been improved approximately five times and more, respectively, compared to that installed on Prius ’97 [9]. On the other hand, although the torque density of each motor has been hardly changed, a reduction gear has enabled to elevate the axle torque necessary for propelling the large vehicles such as RX400h and GS450h. As one of effective strategies for increasing the motor power density, the technological tendency to employ the combination of a high-speed machine and a reduction gear would be accelerated.

In other circumstances, Permanent Magnet Flux Switching Machines (PMFSM) has been a popular research topic due to its high power density and robust rotor structure [10-12]. With both permanent magnets and armature windings located at the stator and robust single piece rotor similar to that of the switched reluctance machine, PMFSM have the advantages of easy cooling of all active parts, and better suitability for high speed drives compared to conventional PM machines.

To provide further attractive characteristics, a new structure of 6-slot 5-pole PMFSM with additional excitation has been proposed by the author as illustrated in Fig. 1. The additional excitation coils are also located at the stator side which gives extra advantage to the machine as a secondary flux sources. On the other hand, the additional excitation on the stator can improve maximum torque and maximum power with the assistance of variable flux control capability [13]. Fig. 2 illustrates the direction of flux paths caused by permanent magnet and mmf of excitation coil in this machine. The presence of excitation coil makes these types of machines more attractive in terms of modulating the permanent magnet flux. Basically, the principle of this machine is similar to 12-slot 10-pole machine discussed in [14-17]. This type of machine is classified into hybrid excitation machines (HEM) which are also becoming more popular over the years [18-20].

After some design refinements and improvements especially on the rotor radius and field excitation slot area, this machine is capable to operate at desired performance. However, the final design of 6-slot 5-pole PMFSM with field excitation shown in Ref [13] has

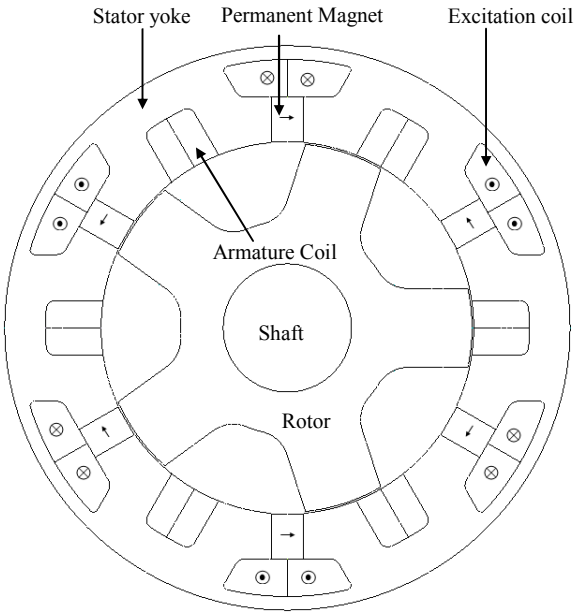

Fig. 1. 6-slot 5-pole Permanent Magnet Flux Switching Machine (PMFSM) with additional field excitation

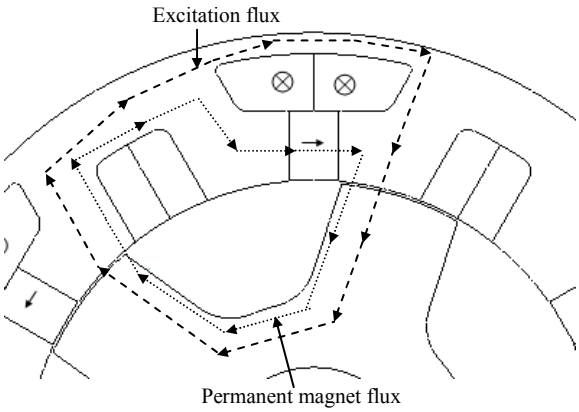

Fig. 2. Flux paths of permanent magnet and excitation coil in 6-slot-5-pole machine

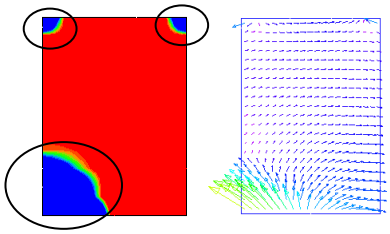

(a) flux density contour (b) flux density vector

Fig. 3. Permanent magnet demagnetization for rotor position at 50° electrical during high temperature (180C°)

limitation of operating in high thermal condition resulting in permanent magnet demagnetization as high as 11.9% as shown in Fig. 3.

This paper presents an investigation into parameter optimization study of 6-slot 5-pole PMFSM with field excitation for traction drives in HEV having permanent magnet volume of 1.0kg and 0.5kg respectively. Some design refinements based on 2D-FEA are conducted to improve the drawback of originally design machine. Moreover, the parameter optimization study is treated to obtain 0% permanent magnet demagnetization at high thermal condition as high as 180C° with better torque-speed characteristics and power production. In addition, a comparison between the rotor mechanical strength, the loss and the efficiency for both condition are also predicted.

II. Design Restriction and Specifications for HEV Applications

The design restrictions and target specifications of the proposed machine for HEV applications are listed in Table I. The table includes the available and estimated specifications of the IPMSM for LEXUS RX400h [21]. The electrical restrictions related with the inverter are set to be much severe. Assuming that only a water cooling system is employed as the cooling system of the machine, the limit of the current density is set to the maximum of $20A_{rms}/mm^2$ for armature winding and $20A/mm^2$ for excitation coil. The outer diameter and the stack length of main part of the target machine are identical with those of IPMSM. Initially, the permanent magnet weight of the design machine is set to 1.0kg and the parameter optimization is made to realize the target performances. Then, the volume of permanent magnet is reduced to 0.5kg and the same method of optimization is treated to the machine.

Since the rotor structure is mechanically robust to rotate at high speed because it consists of only stacked soft iron sheets, the target maximum operating speed is elevated up to 20,000r/min. The target maximum torque 210Nm is determined from a realization of comparable maximum axle torque with the present IPMSM via reduction gear with ratio of 4:1. The maximum power and the target motor weight to be designed are set to be more than 123kW and less than 35kg, resulting in that the proposed machine promises to achieve the maximum power density of 3.5kW/kg similar with the estimate of IPMSM.

Commercial FEA package, JMAG-Studio ver.9.1, released by Japan Research Institute is used as 2D-FEA solver for this design. The permanent magnet material is NEOMAX 35AH whose residual flux density and

TABLE I
PMFSM Design Restrictions and Specifications for HEV Applications.

Items	IPMSM RX400h	PMFSM
Max. DC-bus voltage inverter (V)	650	650
Max. inverter current (A_{rms})	Confidential	240
Max. current density in armature winding, J_a (A_{rms}/mm^2)	Confidential	20
Max. current density in excitation winding, J_e (A/mm^2)	NA	20
Stator outer diameter (mm)	264	264
Motor stack length (mm)	70	70
Shaft radius (mm)	30	30
Air gap length (mm)	0.8	0.8
Permanent magnet weight (kg)	1.1 (estimated)	1.0 / 0.5
Maximum speed (r/min)	12,400	20,000
Maximum torque (Nm)	333	> 210
Reduction gear ratio	2.478	4
Max. axle torque via reduction gear (Nm)	825	> 840
Max. power (kW)	123	> 123
Power density (kW/kg)	3.5	> 3.5

TABLE II
PERMANENT MAGNET DEMAGNETIZATION AT SEVERAL COMBINATIONS OF H_{AG-PM}, H_{E-PM} AND D_4

H_{ag-pm} (mm)	5.0	6.0	7.0
D_4 (mm)	15.0	14.0	13.0
H_{e-pm} (mm)	1.0	1.0	1.0
T (Nm)	191.9	178.7	168.9
r/min	5890	6031	6260
pf	0.62	0.59	0.58
P (kW)	118.4	112.9	110.7
D	1.43%	0%	0%

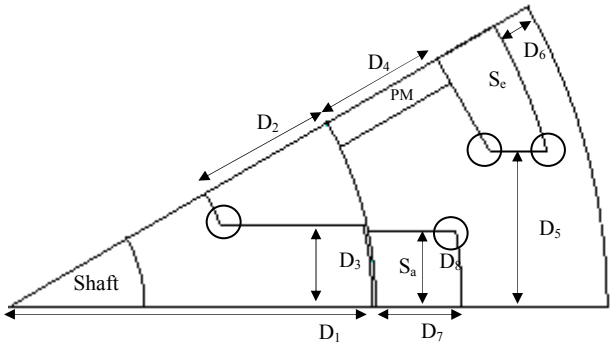

Fig. 4. Design parameters of D_1 to D_8 for 6-Slot 5-Pole PMFSM

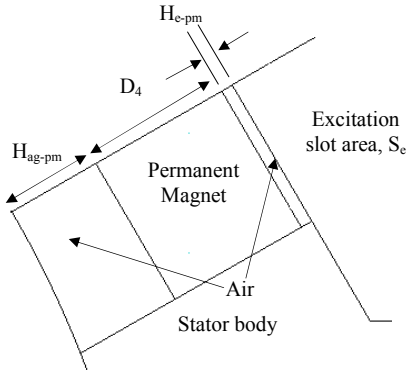

Fig. 5. Additional parameters defined between permanent magnet, inner stator body and inner excitation slot area

coercive force at 20C° are 1.2T and 932kA/m, respectively. The electrical steel, 35H210 is used for rotor and stator body.

III. DESIGN PARAMETERS AND PROCEDURES

Initially, design free parameters D_1 to D_8 are defined as shown in Fig. 4. However, since the demagnetization is located at the upper and lower edges of permanent magnet as shown in Fig. 3, two additional design free parameters i.e., height between air gap and permanent magnet, H_{ag-pm} and height between excitation coil and permanent magnet, H_{e-pm} are defined as illustrated in Fig. 5. The 0% demagnetization is predicted by changing H_{ag-pm}, H_{e-pm}, and D_4 while keeping other parameters constant. It is found that the combination of 6.0mm of H_{ag-pm}, 1.0mm of H_{e-pm} and 14.0mm of D_4 give 0% demagnetization at maximum torque-power of 178.7Nm and 112.9kW respectively as shown in Table II.

Then, the second step is carried out by updating the rotor parameters, D_1, D_2 and D_3 while keeping the other parameters constant. Since the torque increases with the increase in the rotor radius, D_1 is considered as the dominant parameter to improve the maximum torque. The obtained torque characteristic versus D_1 is shown in Fig. 6. The torque is maximized when the rotor radius reaches 88.2mm. Then, keeping D_1 = 88.2mm, the rotor pole depth D_2 and the rotor pole width D_3 are adjusted. Fig. 7 illustrated the torque vs. rotor pole width, D_3 for various rotor pole depths D_2. The torque is maximized when D_2 is 38.2mm and D_3 is 18.5mm, respectively.

The third step of the design is done by changing the excitation slot parameters D_4, D_5 and D_6. Initially, the excitation slot area S_e is determined according to variations of D_4, D_5 and D_6 while keeping the rotor shape parameters and the slot area of armature winding S_a constant. Fig. 8 demonstrates the torque vs. D_5 for different D_4 and D_6. The maximum torque is obtained when D_4 is 12.0mm, D_5 is 35.3mm and D_6 is 9.4mm, respectively.

Then, the fourth step is carried out to the armature slot

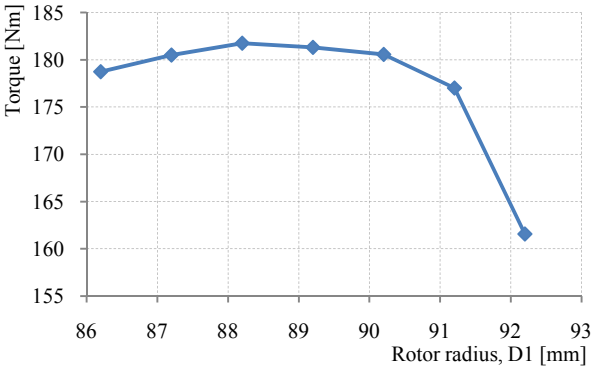

Fig. 6. Torque versus rotor radius D_1 characteristic

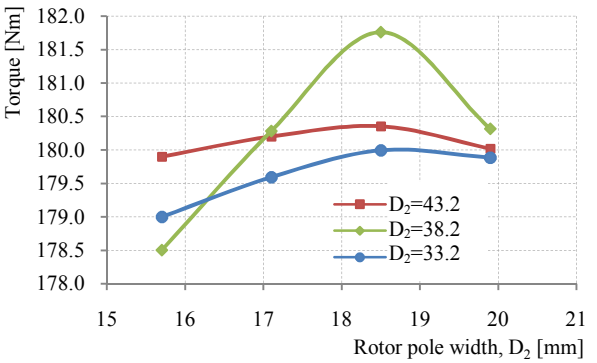

Fig. 7. Torque versus rotor pole width, D_2 for various rotor pole depth, D_3

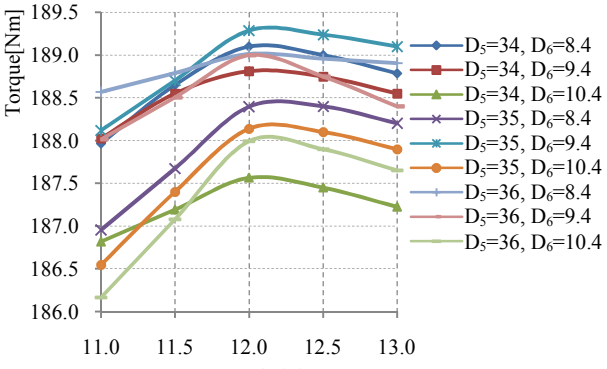

Fig. 8. Torque versus permanent magnet height, D_4 for various excitation coil pitch, D_5 and stator outer core thickness, D_6

area S_a with keeping all parameters discussed above constant. The necessary armature slot area S_a is determined by varying armature coil height, D_7 and armature coil width, D_8 to accommodate integer number of turns, N_a for armature coil. The plot of torque versus N_a is depicted in Fig. 9. The torque and power obtained is well balanced when N_a is 16 turns, D_7 is 27.0mm and D_8 is 13.0mm, respectively.

This design method is treated repeatedly from step 1 to step 4 until the target torque and power are satisfied. The final maximum torque and power achieved are 211.7Nm and 123.1kW respectively which met the target requirements. All design parameters are adjusted with keeping the permanent magnet volume of 1.0kg and air gap length of 0.8mm constant under the maximum current

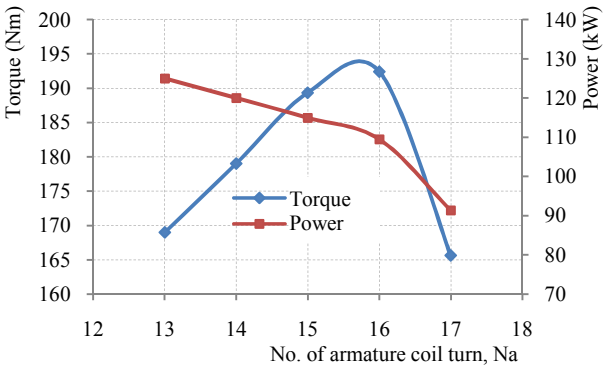

Fig. 9. Torque and power versus number of turns of armature coil

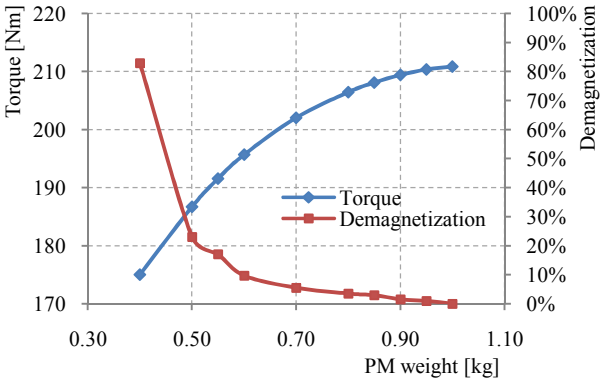

Fig. 10. Torque and demagnetization ratio versus permanent magnet weight

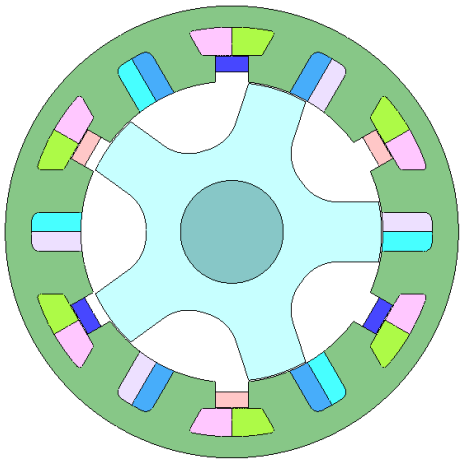

Fig. 11. Final design with 0.5kg permanent magnet

density condition.

In effort to use less-rare-earth magnet, the volume of permanent magnet from the final design above, is reduced to 0.5kg by reducing the permanent magnet width while keeping the $H_{ag\text{-}pm}$ and $H_{e\text{-}pm}$ constant. The performance of the machine with various permanent magnet volumes ranging from 1.0kg to 0.4kg is depicted in Fig. 10. From the figure, the machine having permanent magnet less than 0.4kg is suffered with much demagnetization as high as 83%. Therefore, the minimum 500g of permanent magnet is selected as initial design for the next design motor.

The initial torque and power obtained at this condition are 186.7Nm and 110.7KW with 23% demagnetization which is far from the target requirements. Similarly, the same parameter optimization method discussed above is treated to get optimum torque and power of the new design machine. The final optimum torque achieved is 202.9Nm with 130.5kW power.

At the end of the design stage, the corners circled in Fig. 5 are designed for the flux to flow smoothly and to ensure high mechanical strength of the rotor. The comparison between both designs parameters appear in Table III. The final design of the machines is shown in Fig. 11. The estimated weight of the former machine is 26.2kg and the latter is 26.7kg respectively. It is obvious that the design with fewer magnets has larger stator and rotor volume to keep the same performances.

IV. Design Results and Performance Based on Finite Element Analysis

A. *Torque and Power versus Speed Characteristics*

The torque and power versus speed curves of both designed motor are plotted in Fig. 12. For the design with 1.0kg magnet, the maximum torque obtained at base speed 5,556r/min is 211.7Nm and the corresponding power reaches 123.1kW with the power factor of 0.64. The average power of 131.7kW is achieved between 5,000 - 7,000r/min. The maximum torque density and power density are 8.1Nm/kg and 5.2kW/kg, respectively.

On the other hand, for the design with 0.5kg magnet,

TABLE III
Final Design Parameters

	Details	PMFSM 1.0kg	PMFSM 0.5kg
D_1	Rotor radius (mm)	85.6	87.2
D_2	Rotor pole depth (mm)	37.6	37.2
D_3	Rotor pole width (mm)	14.7	17.46
D_4	Permanent magnet length (mm)	13.8	8.9
D_5	Excitation coil pitch (mm)	35.3	36.3
D_6	Stator outer core thickness (excitation side) (mm)	10.4	12.4
D_7	Armature coil height (mm)	29.26	28.71
D_8	Armature coil width (mm)	12.0	12.98
$H_{ag\text{-}pm}$	Distance between air gap and permanent magnet (mm)	4.5	5.6
$H_{e\text{-}pm}$	Distance between excitation coil and permanent magnet (mm)	0.3	0.5
N_a	No. of turns of armature coil	16	15
D	Demagnetization ratio (%)	0.0	0.0
AT_e	Excitation coil ampere turn (AT)	4501.5	4461.3
S_a	Armature coil area (mm^2)	349.1	327.3
S_e	Excitation coil area (mm^2)	375.1	343.2
T	Torque (Nm)	211.66	202.9
P	Power (kW)	123.1	130.5

the maximum torque obtained at base speed 6,140r/min is 202.9Nm with the power factor of 0.68. The corresponding power reaches 130.5kW which is much higher than the target 123kW power. The average power of 135.5kW is achieved between 5,000 - 7,000r/min. The maximum torque density and power density are 7.6Nm/kg and 5.1kW/kg, respectively, which meet the target requirement for the HEV drive.

B. *Magnet Demagnetization at High Temperature*

The demagnetization of permanent magnet in this machine is defined as the ratio of the volume of permanent magnet demagnetized to the total volume of permanent magnet. The knee point on the demagnetization curve for NEOMAX 35AH is referred to identify whether an element of permanent magnet is demagnetized or not. Fig. 13 illustrates the flux density contour diagram and flux density vector diagram of permanent magnet for rotor position 50° electrical. The calculated results show that the permanent magnet used in this machine has 0% demagnetization even if it is operated at higher temperature as high as 180°C.

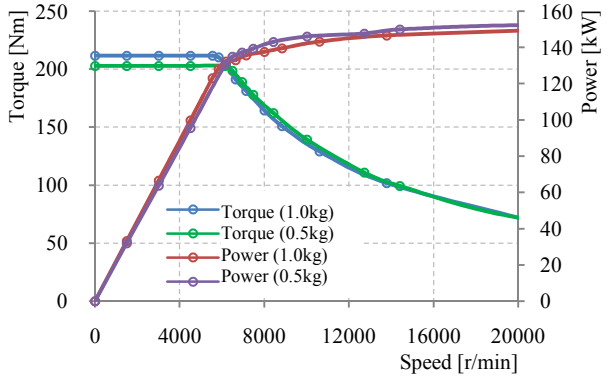

Fig. 12. Torque and power versus speed characteristics

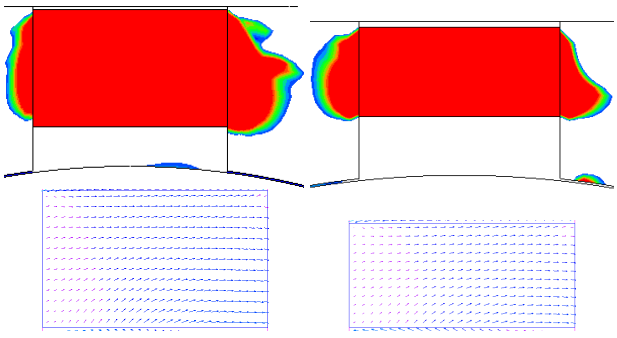

(a) PM=1.0kg (b) PM=0.5kg

Fig. 13. Flux density contour and vector diagram of permanent magnet

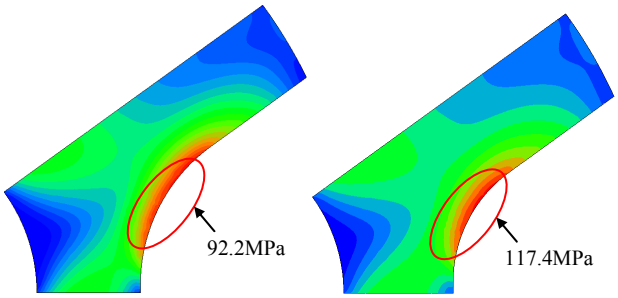

(a) PM=1.0kg (b) PM=0.5kg

Fig. 14. Principal stress distribution of rotor at 20,000r/min

C. *Rotor Stress Prediction at 20,000rpm*

The mechanical stress prediction of the rotor structure at the maximum speed 20,000r/min is executed by centrifugal force analysis based on 2D-FEA. The stress distribution of the rotor is illustrated in Fig. 14. The maximum principal stress for each design are 92.2MPa and 107.4MPa, respectively, which is lower than the original design and much smaller than 300MPa being allowable as the maximum principal stress in conventional electromagnetic steel. This is a great advantage of PMFSM with robust rotor structure that makes it applicable for high-speed application compare to IPMSM.

D. *Motor Loss and Efficiency*

Fig. 15 demonstrates specific frequent operating points of motor under urban-traffic driving situation of HEVs noted as No. 1 to No. 6 for both condition. The motor efficiency under these operating points should be as good as possible because it plays an important role for improving the fuel consumption of vehicles. Motor efficiency in this section is calculated by 2D-FEA considering copper losses in armature winding and iron losses in all laminated cores. The detailed loss analysis and motor efficiency of this machine are listed in Table IV. In the table, P_i is the iron loss, P_c is the copper loss, and P_o is the total output power.

At frequent operating points from No. 1 to No. 6 under relatively low load condition, the proposed machine achieves high efficiency as much as 94.36% to 96.29%. The efficiency is slightly degraded for the machine with 0.5kg permanent magnet because of increasing in rotor and stator volume. Even though the motor efficiency of the latter design is 0.13% - 1.38% lower than that of the former design, the proposed machine can still work at high efficiency as much as 96.11%. The overall

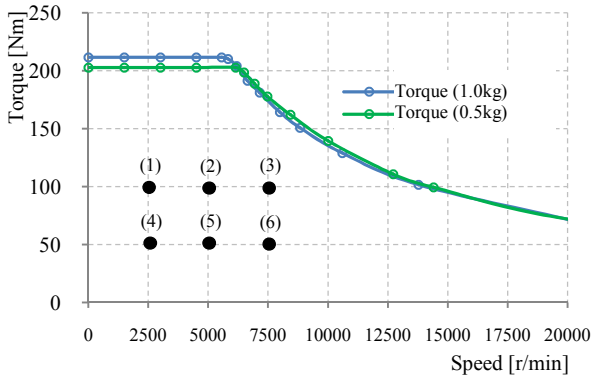

Fig. 15. Frequent operating points for the target HEV drive

TABLE IV
LOSS AND EFFICIENCY OF THE DESIGNED MOTOR OVER OPERATING POINT SHOWN IN FIG. 15.

No.	PM=1.0kg			PM=0.5kg		
	P_c (%)	P_i (%)	P_o (%)	P_c (%)	P_i (%)	P_o (%)
1	2.62	1.67	95.71	2.89	1.69	95.42
2	1.32	2.39	96.29	1.46	2.43	96.11
3	0.88	3.02	96.10	0.97	3.06	95.97
4	2.48	1.89	95.63	3.10	2.54	94.36
5	1.25	2.65	96.10	1.56	3.53	94.91
6	0.83	3.32	95.85	1.04	4.38	94.58

performances of the proposed machine based on finite element analysis are summarized in Table V.

V. CONCLUSIONS

In this paper, the design studies of 6-slot 5-pole PMFSM with field excitation for HEV application have been presented. The method of finding the maximum performance of the machine was clearly demonstrated which has met the target specifications. The demagnetization of permanent magnet at high temperature has also been solved by the proposed method. The goal of this research for an extension in speed and torque ranges has been accomplished. The proposed machine has also reduced the volume of permanent magnet approximately by 50% of that used in existing IPMSM for LEXUS RX400h while keeping the power density intact.

TABLE V
PERFORMANCE OF PMFSM WITH HYBRID EXCITATION

Items	IPMSM	PMFSM	
PM weight (kg)	1.1	1.0	0.5
Max. speed (r/min)	12,400	20,000	20,000
Max. torque (Nm)	333	211.7	202.9
Max. power (kW)	123	123.1	130.5
Reduction gear ratio	2.478	4	4
Max. axle torque via reduction gear (Nm)	825	846.8	811.6
Max. power @6-7kr/min (kW)	123	131.7	135.5
Rotor mechanical stress (MPa)	NA	92.2	117.4
PM demagnetization factor at 180°C (%)	NA	0.00	0.00
Motor efficiency over most of operating region (%)	NA	> 95	> 94
Motor weight (kg)	> 30	26.2	26.7
Power density (kW/kg)	3.5	5.0	5.1
Torque density (Nm/kg)	NA	8.1	7.6

REFERENCES

[1] C. Chan, "The state of the art of electric, hybrid, and fuel cell vehicles," *Proc. IEEE*, vol. 95, no. 4, pp. 704–718, Apr. 2007.

[2] M. Ehsani, Y. Gao, and J. M. Miller, "Hybrid Electric Vehicles: Architecture and Motor Drives," *Proc. IEEE*, vol. 95, no. 4, pp. 719–728, Apr. 2007.

[3] D. W. Gao, C. Mi, and A. Emadi, "Modeling and Simulation of Electric and Hybrid Vehicles," *Proc. IEEE*, vol. 95, no. 4, pp. 729–745, Apr. 2007.

[4] G. Rizzoni, L. Guzzella, and B. M. Baumann, "Unified Modeling of Hybrid Electric Vehicle Drivetrains," *IEEE Trans. on Mechatronics,* vol. 4, no.3 pp. 246–257, Sept 1999.

[5] K. C. Kim, C. S. Jin, and J. Lee, "Magnetic Shield Design Between Interior Permanent Magnet Synchronous Motor and Sensor for Hybrid Electric Vehicle," *IEEE Trans. on Magnetics,* vol. 45, no.6 pp. 2835–2838, June 2009.

[6] K. T. Chau, C. C. Chan, and C. Liu, "Overview of Permanent-Magnet Brushless Drives for Electric and Hybrid Electric Vehicles," *IEEE Trans. on Industrial Electronics,* vol. 55, no.6 pp. 2246–2257, June 2008.

[7] Mineral Resource Information Center affiliated to Japan Oil, Gas and Metals National Corporation, "Metal Resources Report", Vol. 36, No.1, pp.11-16, 2006

[8] T. Kosaka, T. Hirose and N. Matsui, "Brushless Synchronous Machine with Wound-Field Excitation using SMC Core Designed for HEV Drives", Proc. The 2010 International Power Electronics Conference, (IPEC 2010), Sapporo (Japan), June 2010.

[9] R. Mizutani, "The present state and issues of the motor employed in TOYOTA HEVs", Proceedings of the 29th Symposium on motor technology in Techno-Frontier 2009, Session No.E-3-2, pp.E3-2-1-E3-2-20, 2009

[10] Y. Chen, Z. Q. Zhu, and David Howe, "Three-Dimensional Lumped-Parameter Magnetic Circuit Analysis of Single-Phase Flux-Switching Permanent-Magnet Motor" *IEEE Trans. on Industrial Applications,* vol. 44, no.6 pp. 1701–1710, Dec 2008.

[11] Z. Q. Zhu, Y. Pang, D. Howe, S. Iwasaki, R. Deodhar, and A. Pride, "Analysis of electromagnetic performance of flux-switching PM machine by nonlinear adaptive lumped parameter magnetic circuit model" *IEEE Trans. on Magnetics,* vol. 41, no.11 pp. 4277–4287, Nov 2005.

[12] E. Hoang, A. H. Ben-Ahmed, and J. Lucidarme "Switching flux permanent magnet polyphased synchronous machines", Proc. of 7th European Conference on Power Electronics and Applications, vol. 3, 903-908, 1997.

[13] E. Sulaiman, T. Kosaka, and N. Matsui, "Design and Performance of 6-Slot 5-Pole Permanent Magnet Flux Switching Machine with Hybrid Excitation for Hybrid Electric Vehicle Applications", Proc. The 2010 International Power Electronics Conference, (IPEC 2010), Sapporo (Japan), June 2010.

[14] E. Hoang, M. Lecrivain, and M. Gabsi, "A new structure of a switching flux synchronous polyphased machine with hybrid excitation", Proc. of European Conf. on Power Electronics and Appl., No.14, Aalborg, 2007 (CD-ROM, ISBN-9789075815108)

[15] E. Hoang, S. Hlioui, M. Lecrivain, and M. Gabsi, "Experimental comparison of lamination material case switching flux synchronous machine with hybrid excitation" Proc. European Conf. on Power Electronics and Appl., No.53, Barcelona, 2009. (CD-ROM, ISBN-9789075815009).

[16] E. Sulaiman, T. Kosaka, Y. Tsujimori, and N. Matsui, "Performance Analysis of Permanent Magnet Flux Switching Machine with Hybrid Excitation", Proc. International Conf. on Electrical Energy and Industrial Electronics System (EEIES 2009), Malaysia, Dec 2009.

[17] E. Sulaiman, T. Kosaka, Y. Tsujimori, and N. Matsui, "Design of 12-Slot 10-Pole Permanent Magnet Flux Switching Machine with Hybrid Excitation for Hybrid Electric Vehicle", Proc. The 5th IET International Conference on Power Electronics, Machine and Drives (PEMD 2010), Brighton (UK), April 2010.

[18] J. A. Tapia, F. Leonardi and Thomas A. Lipo, "Consequent-pole Permanent Magnet Machine with Extended Field-Weakening Capability", *IEEE Trans. on Industrial Application*, vol. 30, No.6, pp. 1704-1709, 2003.

[19] L.Vido, A. Amara, M. Gabsi, M. Lécrivain and F. Chabot, "Compared Performances of Homopolar and Bipolar Hybrid Excitation Synchronous Machines", Proc. The 40th IEEE/IAS Ann. Meet., pp.1555-1560, 2005

[20] I. Ozawa, T. Kosaka and N. Matsui, "Less Rare-Earth Magnet-High Power Density Hybrid Excitation Motor Designed for Hybrid Electric Vehicle Drives", Proc. European Conf. on Power Electronics and Appl., Barcelona, No.772, 2009 (CD-ROM, ISBN-9789075815009)

[21] M. Kamiya, "Development of Traction Drive Motors for the Toyota Hybrid Systems", *IEEJ Trans. on Industrial Application,* Vol.126, No.4, pp.473-479, 2006. (in English)